Supplementary material of

HailCam: An Automated Imaging System for Real-Time Measurement of Hail Size Distributions and Fall Rates

Baolei Lyu[1,2], Hui Wang[3], Tianlei Gao[1,2], Zhanfu Yin[3], Xiaofeng Lou[3], Yugang Duan[1,2], Yihang Huang[1,2], Zhiqiang Zhao[3]

[1] Huayun Sounding Meteorological Technology Co. Ltd, Beijing, 102200, China

[2] Key Laboratory of Intelligent Meteorological Observation Technology, Beijing 100081, China

[3] CMA Key Laboratory of Cloud-Precipitation Physics and Weather Modification (CPML), CMA Weather Modification Centre (WMC), Beijing 100081, China

Correspondence to: Baolei Lyu (baoleilv@foxmail.com), Hui Wang(hwang@cma.gov.cn), Zhanfu Yin (yin_zf@126.com)

Text S1. Metric Reconstruction of Planar Objects from a Calibrated Camera

We aim to recover the true physical dimensions of a rectangular sub-region observed in a single image of a planar calibration target (a square of known side length L).

S1.1 Coordinate System and Geometry

- The world coordinate system is defined such that the calibration square lies on the plane $Z=0$, centered at the origin.
- The four corners of the square have world coordinates:

$\boldsymbol{P}1 = (-L/2, -L/2, 0)^{\top}, \boldsymbol{P}2 = (L/2, -L/2, 0)^{\top}, \boldsymbol{P}3 = (L/2, L/2, 0)^{\top}, \boldsymbol{P}4 = (-L/2, L/2, 0)^{\top}.$

S1.2 Camera Model

The pinhole camera model relates a 3D world point $\mathbf{P}=[X,Y,Z,1]^{\top}$ to its image projection $\mathbf{p}=[u,v,1]^{\top}$ (in homogeneous coordinates) via:

$$\boldsymbol{p} \sim \boldsymbol{K}[\boldsymbol{R} \mid \boldsymbol{t}]\boldsymbol{P},$$

where:

- $\boldsymbol{K} \in R3 \times 3$ is the intrinsic matrix (containing focal length, principal point, and skew),
- $\boldsymbol{R} \in SO(3)$ and $\boldsymbol{t} \in R3$ are the extrinsic rotation and translation.

Since all points of interest lie on $Z=0$, the projection simplifies to a planar homography.

S1.3 Homography Computation

For points on the $Z=0$ plane, the mapping reduces to:

$\boldsymbol{p} \sim \boldsymbol{H}XY1$, where $\boldsymbol{H} = \boldsymbol{K}[\boldsymbol{r}_1 \boldsymbol{r}_2 \boldsymbol{t}]$,

and $\boldsymbol{r}_1$,$\boldsymbol{r}_2$ are the first two columns of $\mathbf{R}$.

S1.4 Inverse Projection of Region of Interest

Let $\boldsymbol{p}_i = (u_i, v_i)^{\top}$ (i=1,…,4) denote the detected image corners of the small rectangle. After radial/tangential distortion correction, each point is converted to normalized image coordinates and then back-projected:

$X_i Y_i w_i = \boldsymbol{H} - u_i v_i 1, (x_i, y_i) = (w_i X_i, w_i Y_i).$

Assuming consistent corner ordering (e.g., counter-clockwise), the physical width W and height H are:

$W = (x_2 - x_1)^2 + (y_2 - y_1)^2, H = (x_4 - x_1)^2 + (y_4 - y_1)^2.$

S1.5 Unknown Extrinsic Parameters

Considering that $\mathbf{R}$ and $\mathbf{t}$ are not available, they can be estimated by detecting the four corners of the full reference square in the image and solving the PnP problem:

$\{\boldsymbol{R}, \boldsymbol{t}\} = solvePnP(\{\boldsymbol{P}i\}, \{\boldsymbol{p}i\}, \boldsymbol{K}, \boldsymbol{\xi})$,

where $\boldsymbol{\xi}$ denotes distortion coefficients. Standard algorithms (e.g., EPnP, iterative Levenberg–Marquardt refinement) yield sufficient accuracy for our application.

S1.6 Practical Considerations

Image points must be undistorted before homography inversion. It must be consistent between image and world frames. Unit consistency should be ensured that t and L must share the same unit (e.g., meters). Limited by calibration precision, corner detection sub-pixel error (<0.1 px), and planarity assumption. This pipeline enables accurate, traceable conversion from pixel measurements to physical dimensions, forming the basis for hail size quantification in our system.

Text S2: Quantitative Error Analysis

In this method, deep learning image recognition technology was utilized to observe and systematically analyze hail data. While the experimental results demonstrate the effectiveness and practicality of the proposed method, inevitable errors still occur. To ensure the reliability of the experimental results, it is essential to deeply analyze the causes of these errors. This section will discuss and analyze the factors that contributed to the discrepancies between the experimental results and theoretical values. Analyzing these sources of error will help improve the accuracy and reliability of hail observations, as well as provide ideas for reducing errors in future experiments.

S2.1 Errors by Equipment Installation

In Section 2.2 the calculation steps for detecting hail particles via captured images were detailed. However, all the derivations were grounded on the following assumptions. First, the hail collection plane is absolutely parallel to the image coordinate system of the captured image. Second, the camera captures the entire surface of the collection platform. Lastly, the camera is precisely focused for accurate imaging.

S2.1.1 Distortion of Hail Collection Platform

When the hail collection platform is depicted in the image acquired through the camera, as shown in Figure 4.1, there is a rotation of the hail collection platform relative to the image coordinate system $u - O_{uv} - v$, meaning it is not parallel to u-O-v and has a rotation angle α. If $v_A < v_B$, the platform tilts to the left; if $v_A > v_B$, the platform tilts to the right, with a tilt angle $\alpha < 90°$. The coordinates of points should be corrected from $A(u_A, v_A)$, $B(u_B, v_B)$, $C(u_C, v_C)$, $D(u_D, v_D)$ to $A'(u'_A, v'_A)$, $B'(u'_B, v'_B)$, $C'(u'_C, v'_C)$, $D'(u'_D, v'_D)$.

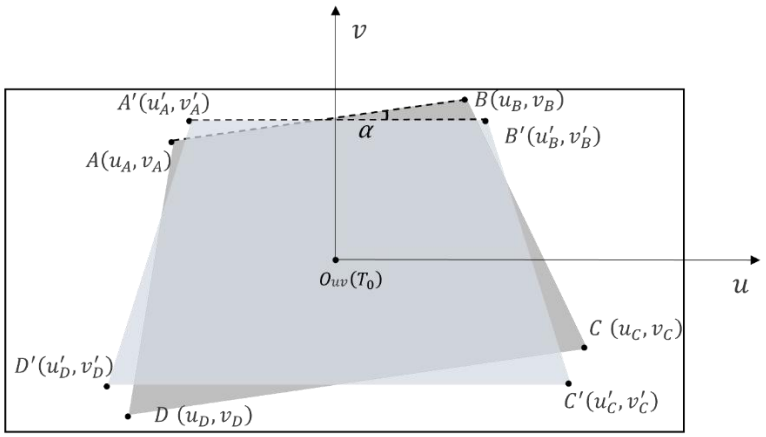

Figure S1: Schematic of the hail collection platform when it is tilted, where α is the tilt angle and A, B, C, D are the four vertices of the collection platform in the image.

To correct for this, we rotate the origin O_{uv} by angle α, defining the rotation matrix R_O:

$$R_O = \begin{bmatrix} cos\ \alpha & -sin\ \alpha \\ sin\ \alpha & cos\ \alpha \end{bmatrix} \quad (4.1)$$

For any point Q rotated around point O_{uv} by angle α, the new point Q' is given by:

$$\begin{bmatrix} u'_Q \\ v'_Q \end{bmatrix} = R_S \begin{bmatrix} u_Q \\ v_Q \end{bmatrix} \quad (4.2)$$

From Figure 4.1, the expression for α can be obtained as follows:

$$\sin\alpha = \frac{u_B - u_A}{\sqrt{(u_B - u_A)^2 + (v_B - v_A)^2}}$$
$$\cos\alpha = \frac{v_B - v_A}{\sqrt{(u_B - u_A)^2 + (v_B - v_A)^2}} \quad (4.3)$$

Substituting these expressions into Equation 4.2, obtaining the coordinates for points $A'(u'_A, v'_A)$, $B'(u'_B, v'_B)$, $C'(u'_C, v'_C)$ and $D'(u'_D, v'_D)$ as follows:

$$\begin{bmatrix} u'_A \\ v'_B \end{bmatrix} = \begin{bmatrix} u_A \cdot cos\ \alpha - v_A \cdot sin\ \alpha \\ u_A \cdot sin\ \alpha + v_A \cdot cos\ \alpha \end{bmatrix}$$
$$\begin{bmatrix} u'_B \\ v'_B \end{bmatrix} = \begin{bmatrix} u_B \cdot cos\ \alpha - v_B \cdot sin\ \alpha \\ u_B \cdot sin\ \alpha + v_B \cdot cos\ \alpha \end{bmatrix}$$
$$\begin{bmatrix} u'_C \\ v'_C \end{bmatrix} = \begin{bmatrix} u_C \cdot cos\ \alpha - v_C \cdot sin\ \alpha \\ u_C \cdot sin\ \alpha + v_C \cdot cos\ \alpha \end{bmatrix} \quad (4.4)$$
$$\begin{bmatrix} u'_D \\ v'_D \end{bmatrix} = \begin{bmatrix} u_D \cdot cos\ \alpha - v_D \cdot sin\ \alpha \\ u_D \cdot sin\ \alpha + v_D \cdot cos\ \alpha \end{bmatrix}$$

Subsequently, substitute the coordinates of points $A'(u'_A, v'_A)$, $B'(u'_B, v'_B)$, $C'(u'_C, v'_C)$, $D'(u'_D, v'_D)$ into equation 2.13, replacing points $A(u_A, v_A)$, $B(u_B, v_B)$, $C(u_C, v_C)$, $D(u_D, v_D)$, to derive the modified parameters k'_1 and k'_2:

$$k'_1 = \frac{(v'_D - v'_A)W}{u'_C - u'_D + u'_A - u'_B}$$
$$k'_2 = \frac{u'_B v'_D + u'_D v'_A - u'_A v'_D - u'_C v'_A}{u'_C - u'_D + u'_A - u'_B} \quad (4.5)$$

The error Δd_j between the distance calculated using the coordinates $A'(u'_A, v'_A)$, $B'(u'_B, v'_B)$, $C'(u'_C, v'_C)$, $D'(u'_D, v'_D)$ and the original coordinates $A(u_A, v_A)$, $B(u_B, v_B)$, $C(u_C, v_C)$, $D(u_D, v_D)$ can be expressed as:

$$\Delta d_j = \frac{k_1(u_{j_2} - u_{j_1})}{v_{j_2} + v_{j_1} + 2k_2} - \frac{k'_1(u_{j_2} - u_{j_1})}{v_{j_2} + v_{j_1} + 2k'_2} \quad (4.6)$$

The average error is expressed as:

$$\Delta\bar{d} = \frac{1}{N}\sum_{j=1}^{N} \Delta d_j \quad (4.7)$$

Using Python, 20 sets of $ABCD$ coordinates were randomly generated to simulate the edges of the hail collection platform under real conditions. The rotation angle α was increased by 1° for each calculation. The calculated error Δd_j was computed and displayed in Figure S2. The results indicate that when $0° < \alpha < 45°$, Δd_j<0, the observed diameter is smaller than the actual value. When $45° < \alpha < 90°$, Δd_j becomes more dispersed. In practical situations, the tilt of the collection platform is usually small (i.e., $\alpha < 45°$), resulting in Δd_j being negative, leading to the observed diameter being smaller than the actual diameter.

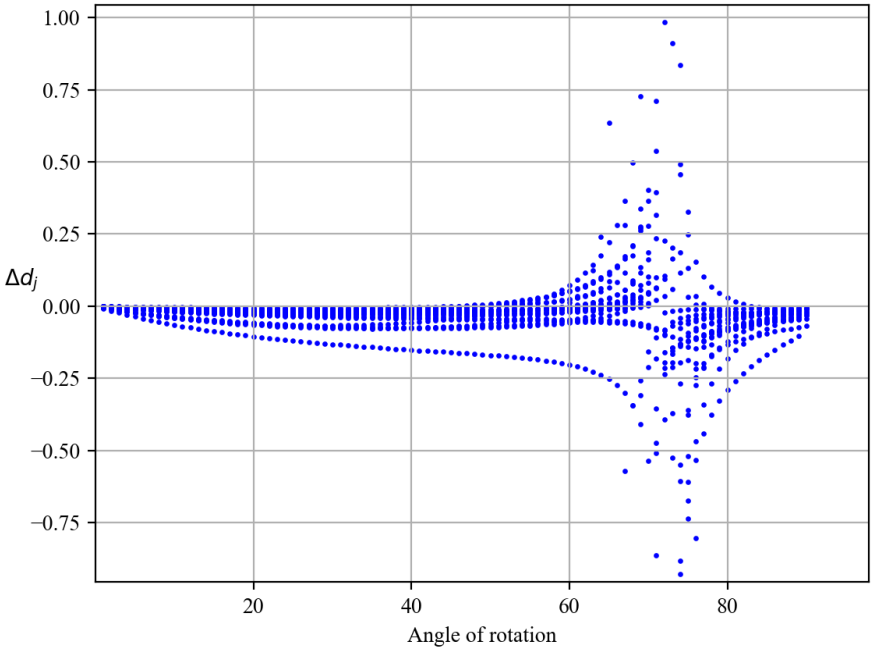

Figure S2: Error analysis for 20 randomly generated sets of A, B, C, D coordinates and rotation angles α, calculated in increments of 1°.

S2.1.2 Incomplete of Hail Collection Platform

Figure S3 illustrates the case where the camera fails to capture the entire collection platform. Since the diameter and algorithm are calculated based on the platform's size and corresponding coordinates in the image, incomplete capture leads to inaccuracies in defining the platform's dimensions and affects the observed hail diameter.

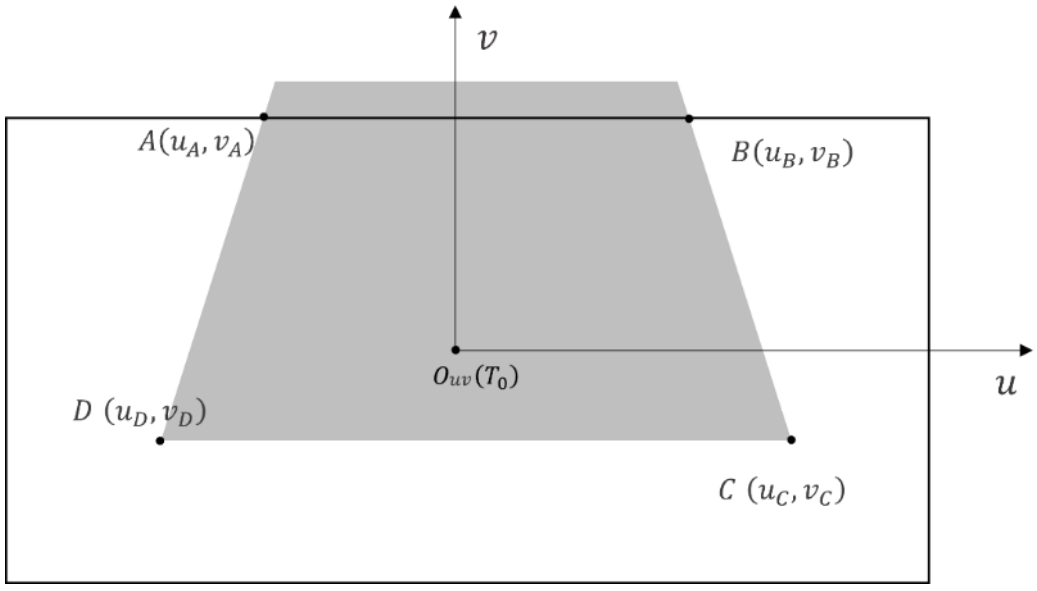

Figure S3: Schematic of incomplete imaging of the collection platform by the camera.

Establishing an installation procedure is then strictly followed to avoid potential installation errors. This procedure should include the following aspects. Camera angle should be carefully calculated and adjusted to ensure coverage of the necessary monitoring area. Focal length of the camera should be optimized according to specific needs to ensure clear image quality.

What’s more, the hail collection platform should be placed correctly within the camera's field of view and keep it level to avoid any tilt. These standardized installation steps will effectively reduce errors caused by improper setup and improve the efficiency and accuracy of the observation system.